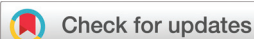


## PAPER

Cite this: *Nanoscale*, 2021, **13**, 3252

# Influences of dynamic and static disorder on the carrier mobility of BTBT-C12 derivatives: a multiscale computational study†

Xingliang Peng, Qikai Li and Zhigang Shuai \*

The role of dynamic and static disorder has been widely discussed for carrier transport in organic semiconductors. In this work, we apply a multiscale approach by combining molecular dynamics simulations, quantum mechanics calculations and kinetic Monte-Carlo simulations to study the influence of dynamic and static disorder on the hole mobility of four didodecyl[1]benzothieno[3,2-*b*]benzothiophene (BTBT-C12) isomers. It is found that the dynamic disorder of transfer integral tends to decrease the mobility for quasi-1D (quasi one-dimensional) BTBT1 and BTBT4 isomers and increase the mobility for 2D (two-dimensional) BTBT2 and BTBT3 isomers, while the dynamic disorder of site energy tends to decrease mobility for all the four isomers; however, the reduction in 2D molecules is much less than that in quasi-1D molecules. Results show that trap defects could reduce the mobility for both the quasi-1D and 2D molecular structures significantly, even to several orders of magnitude. In addition, our work also reveals that there might exist two kinds of oxidation defects of the scatter type for the concerned isomers, which thus leads to greater reduction in mobility for the quasi-1D molecular structures than the 2D molecular structures. The study shows that the 2D molecular structures are favored over the quasi-1D or 1D molecular structure, and it is expected that these results could be used to shed light on device design in organic electronics.

Received 22nd November 2020.

Accepted 14th January 2021

DOI: 10.1039/d0nr08320h

rsc.li/nanoscale

## 1. Introduction

In recent decades, organic semiconductors have been widely used in organic field-effect transistors (OFETs), organic light-emitting diodes (OLEDs), and organic photovoltaic cells (OPVs).<sup>1–3</sup> The performances largely depend on the charge transport in organic active layers. The carrier transport mechanism of the charge transport has been a long standing issue of interest after decades of efforts,<sup>4–7</sup> and the complexity makes it remain a great challenge to understand the behaviors of charge transport.<sup>8–10</sup>

[1]Benzothieno[3,2-*b*]benzothiophene (BTBT) derivatives have been very popular in recent years due to their strikingly high charge carrier mobility.<sup>11,12</sup> The reported BTBT structures with high mobility<sup>13–17</sup> usually have alkyl chains or benzene substituted on the second position of the benzene ring, such as BTBT2 as shown in Fig. 1. Several studies have also been carried out on the influence of different alkyl side-chains on

mobility,<sup>17</sup> and the longer side-chain tends to enhance the mobility because of the stronger or more balanced intermolecular charge transfer and weaker electron–photo coupling.<sup>18</sup> Recently, Tsutsui and co-workers<sup>16</sup> have studied the mobility of four BTBT isomers (Fig. 1) which differ in the position of the substituted  $-C_{12}H_{25}$  alkyl chain, and the results showed that the mobility of BTBT2 is hundreds to thousands of times larger than those of the other three isomers. However, theoretical calculations by both the hopping model and the band theory showed that the mobility difference is only of several

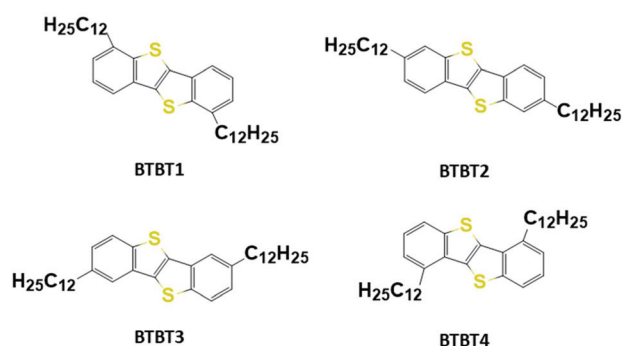


Fig. 1 Chemical structures of the four BTBT isomers.

MOE Key Laboratory of Organic Optoelectronics and Molecular Engineering, Department of Chemistry, Tsinghua University, Beijing 100084, People's Republic of China. E-mail: zgshuai@tsinghua.edu.cn

†Electronic supplementary information (ESI) available. See DOI: 10.1039/d0nr08320h

times. What leads the unpredicted large difference in experimental results is unclear. Could it be the dynamic and static disorder, which is not taken into account in earlier theoretical calculations, leading to the difference in BTBT2 and other isomers?

In organic semiconductors, molecules are packed up by weak van der Waals interactions, which tends to result in large intermolecular displacements (it can be up to 0.5 Å at room temperature<sup>19</sup>). The intermolecular displacement caused by thermal motion consequently leads to fluctuation or the so-called dynamic disorder in the intermolecular transfer integral, which could be often in the same order of magnitude as that of the transfer integral itself,<sup>20</sup> and thus cannot be ignored. The previous study<sup>21</sup> by our group from a tunneling enabled hopping calculation indicated that such a type of dynamic disorder tends to reduce the mobility at lower temperature but to enhance the mobility at room temperature. Specifically, the influence is marginal. In contrast, some studies stated that the dynamic disorder is the major factor to limit the charge transport,<sup>22–24</sup> which can rationalize a number of experimental observations of the “bandlike” decreasing temperature behavior of mobility ( $d\mu/dT < 0$ ). We noted that the quantum nuclear tunneling demonstrated such decreasing temperature dependence from a localized charge.<sup>25</sup> Fratini and co-workers proposed transient localization theory (TLT), in which the disorder is the origin of transient localization length and mobility.<sup>10</sup> Recently, more general methods applicable at different charge transport regimes indicate the non-unique influence of the dynamic disorder on mobility.<sup>26–28</sup> Earlier studies in our group based on the hopping model found that the dynamic disorder drastically reduces mobility for a one dimensional (1D) material, but it has no significant influence for two dimensional (2D) materials.<sup>29</sup>

The molecular thermal vibration induces not only the dynamic off-diagonal disorder (transfer integral), but also the dynamic diagonal disorder, which reflects the fluctuation in

site energy. Earlier simulations usually described the energetic disorder *via* the Gaussian Disorder Model (GDM)<sup>30</sup> as well as its extensions and modifications,<sup>31</sup> and the corresponding standard deviations are around 0.1 eV.<sup>9</sup> This disorder is often considered by calculating the hopping rate with the Miller–Abrahams formalism<sup>32</sup> or Marcus theory,<sup>33</sup> and the degree of the disorder is adjusted by the standard deviation.<sup>34,35</sup> Recent studies present the distribution of site energy by using molecular dynamic (MD) simulations combined with quantum mechanics calculations<sup>31,36,37</sup> and conclude that the dynamic disorder does not depend significantly on the intermolecular interactions but is primarily driven by electronic couplings with intramolecular vibrations.

Even in ordered crystals, in addition to the dynamic disorder, the static disorder arising from defects or impurities

could not be ignored.<sup>9</sup> The origin of defects can vary vastly, such as chemical defects produced by chemical reactions with oxygen or water, or the side products of the chemical synthesis, or structural defects like dislocation as well as grain boundary.<sup>38–41</sup> Studies<sup>42</sup> on pentacene single crystals showed that by taking pentacene–quinone molecules as the main defects, a decrease in the defect concentration from ~0.7% to 0.07% could improve the hole mobility of pentacene single crystals up to 35 cm<sup>2</sup> V<sup>-1</sup> s<sup>-1</sup>. The effects of defects are based on the energy levels of Frontier molecular orbitals (the HOMO and LUMO); when the energy level is located between the HOMO and LUMO of a pure molecule, it acts as a trap, otherwise it acts as a scatter.<sup>43,44</sup> Recent studies suggest that the trap in polymers is most likely related to hydrated oxygen complexes,<sup>45</sup> and also indicate that the trap is of the dielectric effect of water penetrating nano voids, and the trap energy calculated by the empirical rule lies in the range of ~0.3–0.4 eV higher than the HOMO or lower than the LUMO.<sup>46</sup>

In this work, the dynamic disorder of transfer integral and site energy, as well as the static disorder of defects are considered separately in calculations of mobility for the four BTBT isomers; in addition, the influence of disorder on mobility with various 1D or 2D stackings for the concerned isomers is also investigated. Mobility is calculated by employing molecular dynamic (MD) simulations, quantum mechanics calculations and kinetic Monte-Carlo simulations, while the intermolecular hopping rates are calculated based on the Marcus theory and quantum nuclear tunneling method.

## 2. Methodological approach

### 2.1 Mobility calculations

The intermolecular charge transfer rate between two equivalent molecules using the quantum nuclear tunneling model<sup>6</sup> is expressed as:

$$k = \frac{V^2}{\hbar} \int_{-\infty}^{\infty} dt \times \exp \left\{ i\omega t - \sum_j S_j [(2n_j + 1) - n_j e^{-i\omega_j t} - (n_j + 1) e^{i\omega_j t}] \right\} \quad (1)$$

where  $\omega_j$ ,  $S_j$ , and  $n_j = 1/[\exp(\omega_j/k_B T) - 1]$  are the intramolecular vibration frequency, the corresponding Huang–Rhys factor and the occupation number for the  $j$ -th vibrational mode, respectively.  $V$  and  $\omega$  are the transfer integral between two interaction molecules and their energy difference, the latter is taken as zero for the mono-molecular crystal system. In the limit of strong coupling with  $\sum_j S_j \gg 1$ , the short time approximation

$\exp(i\omega t) = 1 + i\omega t + (i\omega t)^2/2$  can be applied. Besides, in the case of high temperature approximation with  $\hbar\omega_j/k_B T \ll 1$ , the occupation number of phonons  $n_j \approx k_B T/\hbar\omega_j$ , and thus the rate equation reduces to the Marcus equation:

$$k = \frac{V^2}{\hbar} \sqrt{\frac{\pi}{\lambda k_B T}} \exp \left[ -\frac{(\Delta G + \lambda)^2}{4\lambda k_B T} \right] \quad (2)$$

where the total reorganization energy  $\lambda = \sum_j \lambda_j = \sum_j S_j \hbar \omega_j$ , and  $\Delta G$  is the site energy difference. The transfer integral  $V$  between molecules  $m$  and  $n$  is calculated with the site-energy overlap correction method:<sup>47</sup>

$$V_{mn} = \frac{V_{mn}^0 - \frac{1}{2}(e_m + e_n)S_{mn}}{1 - S_{mn}^2} \quad (3)$$

here  $e_m = \Phi_m |H| \Phi_m$ ,  $V_{mn}^0 = \Phi_m |H| \Phi_n$ , and  $S_{mn} = \Phi_m |S| \Phi_n$ , where  $\Phi_{m(n)}$  is the Frontier molecular orbital of an isolated molecule  $m(n)$  in the dimer representation, and  $H$  and  $S$  are the dimer Hamiltonian and overlap matrices, respectively.

Based on the above-mentioned methods, the charge hopping rate of two neighboring molecules is calculated. Later on, the kinetic Monte Carlo (KMC) simulations are performed to evaluate the charge diffusion coefficient. For the  $\alpha$ -th pathway, charge hops from molecule  $m$  to molecule  $n$  with probability  $p_\alpha = k_{mn}^\alpha / \sum k_{mn}^\alpha$ , and the simulation time is defined as  $1 / \sum_\alpha k_{mn}^\alpha$ , where  $k_{mn}^\alpha$  is the charge hopping rate obtained from the previous step. By averaging over 2000 trajectories, for example, the diffusion coefficient can be evaluated by:

$$D = \frac{1}{2n} dl(t)^2 / dt \quad (4)$$

where  $n$  is the spatial dimension and  $l(t)$  is the distance of carrier's diffusion. Finally, the carrier mobility can be obtained via the Einstein relationship:

$$\mu = eD / (k_B T) \quad (5)$$

For a crystal, the average mobility ( $\mu_{\text{ave}}$  in Table 2) is obtained by setting the dimension  $n = 3$  and setting  $l(t)$  to the distance of carrier's diffusion in the three dimensional space, and the mobilities along the crystal axis  $a$ ,  $b$  and  $c$  ( $\mu_a$ ,  $\mu_b$  and  $\mu_c$ ) are obtained by setting the dimension  $n = 1$  and setting  $l(t)$  to the distance of carrier's diffusion along the crystal axis  $a$ ,  $b$  and  $c$ .

The mobility calculations are performed by using our home-built MOMAP software.<sup>48</sup> Evaluations of transfer integral are performed at the PW91PW91/6-31G\* level, and the vibrational mode analysis for reorganization energy calculations are based on the configurations obtained by quantum mechanical and molecular mechanical calculations (QM/MM) (the ONIOM models are shown in Fig. S1†), where the central molecule (free) is treated by QM (B3LYP/6-31G\*) and the surrounding molecules (fixed) are treated by MM (UFF). The reorganization energies are obtained by performing geometry optimization and vibrational mode analysis at the B3LYP/6-31G\* level. All the calculations on geometry optimization and frequency calculations are carried out by using the Gaussian 09 program (version E.01).<sup>49</sup> Each kMC simulation is performed with a simulation time of 1 ms, and 2000 simulations are performed for each mobility calculation.

## 2.2 Simulations of dynamic disorder

The fluctuations of transfer integral and site energy are produced by using molecular dynamic (MD) simulations. For each BTBT molecule, a supercell ( $10 \times 4 \times 1$ ,  $5 \times 4 \times 2$ ,  $2 \times 10 \times 2$ , and  $2 \times 10 \times 2$  for BTBT1, BTBT2, BTBT3 and BTBT4 respectively) containing a total of 80 molecules is built based on the crystal structures reported from the experiment.<sup>16</sup> The general AMBER force field (GAFF)<sup>50</sup> is used, and the restrained electrostatic potential (RESP)<sup>51,52</sup> partial charge is used in fitting of the charge parameters for the force field. GROMACS software (version 2019.3)<sup>53</sup> is used to do the MD runs, which has been proven to be efficient for organic small molecules.<sup>54,55</sup> The NPT ensemble at room temperature and ambient pressure is employed for MD simulations, and the time step used is 1 fs. The velocity rescaling thermostat<sup>56</sup> and the Berendsen barostat<sup>57</sup> are used to control the temperature and pressure respectively. The periodic boundary conditions are applied, and a cutoff of 1.2 nm is used to limit the van der Waals interaction, and the particle mesh Ewald (PME) method is used for calculations of electrostatic interactions with a cutoff of 1.2 nm. The total simulation time is set to 1 ns, and the dynamic trajectories are extracted every 20 fs after thermal equilibration of 600 ps with a total of 2050 snapshots.

Once the various trajectory snapshots are obtained, we can continue to do the calculations. For each snapshot, the transfer integrals of several typical dimers (as shown in Fig. 2) at one site are calculated at the PW91PW91/6-31G\* level. For each dimer, the discrete Fourier transformation is performed to get the time-dependent transfer integral fluctuation, and the transfer integral  $V_{mn}(t)$  is expressed by

$$V_{mn}(t) = V_{mn} + \sum_{k=1}^{N-1} \text{Re}V_k \cos(\omega t + \varphi_0) + \sum_{k=1}^{N-1} \text{Im}V_k \sin(\omega t + \varphi_0) \quad (6)$$

where  $N$  is the total number of MD snapshots (2050 in this work),  $V_{mn}$  is the average transfer integral for each dimer,  $\text{Re}V$  and  $\text{Im}V$  are the real part and imaginary part of Fourier coefficients respectively, and  $\varphi_0$  is a random phase factor. In kMC calculations, the transfer integrals of intra-layer dimers are obtained from  $V_{mn}(t)$ , while the transfer integrals of inter-layer dimers (usually has a value of around  $10^{-5}$ – $10^{-6}$  eV) are set to values from crystal structure calculations. It should be noted that, for the dimers with equivalence related positions, they have the same transfer integral fluctuation amplitude; however, the values may still vary due to a different phase factor  $\varphi_0$  as indicated in eqn (6).

For the hole transport in this work, the site energy difference is defined as the difference of the ability to ionize an electron in two sites. Here, in order to speed up the calculations, we applied the Koopmans' theorem and approximated the site energy with the energy of the highest occupied molecular orbital (HOMO) of a molecule. Studies showed that the surrounding molecular environment has no significant effect on the dynamic disorder of HOMO energy;<sup>36,37</sup> thus, we select one molecule from each snapshot to carry out the calculations. The HOMO energy is calculated at the PW91PW91/6-31G\* level, and the site energy difference is obtained from the difference of two randomly

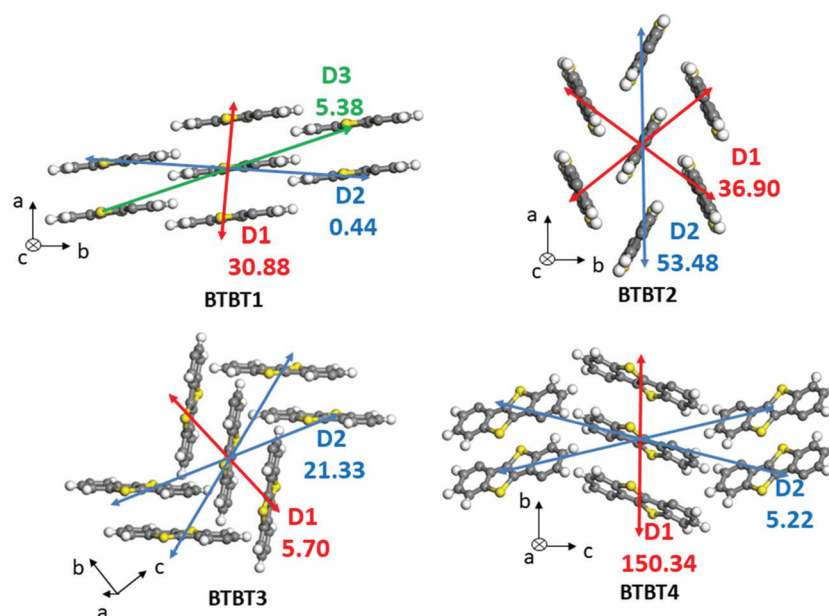


**Fig. 2** The six intra-layer nearest neighbor charge hopping pathways for BTBT isomer crystals and the corresponding transfer integral (unit in meV) calculated at the PW91PW91/6-31G\* level (the alkyl chains are omitted for clarity).

selected HOMO energies. When the sampling is enough, the distribution of site energy difference features a typical Gaussian distribution; in this work, we set up 100 000 samples to approach the Gaussian distribution (as shown in Fig. 5b).

### 2.3 Simulations of the static disorder of defects

We assume that the defects are uniformly distributed in the bulk of materials with a defect ratio. In a kMC run, for all neighboring sites, a random number uniformly distributed between 0 and 1 is generated, and if this value is less than the defect ratio, then the site is set as a defect, otherwise the site is set as a normal molecule. For simplicity, we consider only the transport within the layer, and an electric field is applied along the direction with maximum transfer integral, such as lattice direction *a* for BTBT2 and lattice direction *b* for BTBT4 (the lattice directions are shown in Fig. 2). The electric field is usually taken to be in the range of  $10^4$  to  $10^6$  V cm<sup>-1</sup>,<sup>9</sup> and here, we set the electric field strength to be  $10^6$  V cm<sup>-1</sup>, which contributes less than 0.1 eV (the intermolecular distance is on the order of 1 nm) to the site energy difference. The kMC simulations were run until a charge travels a distance of 100 micrometers at the direction of the applied electric field. The mobility is calculated as:  $\mu = d/(\tau F)$ , where *d* is the distance traveled by the charge,  $\tau$  is the total time, and *F* is the magnitude of applied electric field. The final mobility is the average of a total of 20 simulations.

## 3. Results and discussion

### 3.1 Pure crystal case

Reorganization energy and transfer integral are the two most important parameters that affect the electron transfer rates

among molecules. The hole reorganization energies of the four BTBT isomers are listed in Table 1. It is clear that the four isomers have similar reorganization energy in the range of 220–250 meV in the gas phase, which is consistent with previously reported results.<sup>16</sup> These reorganization energies by summing over all the normal mode relaxation energies are very close to those calculated from the four-point energy methods which are 229, 246, 231, and 232 meV for BTBT1, BTBT2, BTBT3 and BTBT4 respectively, indicating that the harmonic oscillator approximation is appropriate. In the crystal phase, as the molecular vibration is restricted, the reorganization energies decrease slightly by about 3–11 meV, which are quite agreeable to 224, 235, 228, and 229 meV for BTBT1, BTBT2, BTBT3, and BTBT4 respectively. The contributions of vibration modes to geometry relaxation are shown in Fig. S2 and S3,<sup>†</sup> and there exists no significant difference in the gas state and crystal state. Considering the solid system in reality, the reorganization energy of the crystal state is used in the following calculation of the hole hopping rate.

For each BTBT isomer, the HOMO is mainly distributed on the benzothiophene ring (Fig. S4<sup>†</sup>); hence, the transfer integral is mainly related to the relative position of benzothiophene

**Table 1** The hole reorganization energies (meV) of four BTBT isomers obtained by summing over all the normal modes

|                      | BTBT1 | BTBT2 | BTBT3 | BTBT4 |
|----------------------|-------|-------|-------|-------|
| Gas <sup>a</sup>     | 229   | 246   | 231   | 232   |
| Crystal <sup>b</sup> | 224   | 235   | 228   | 229   |

<sup>a</sup> Single molecule (B3LYP 6-31G\*). <sup>b</sup> QM/MM method (B3LYP 6-31G\*/UFF) based on the crystal structure.

rings. The crystal structure of each isomer shows a lamellar packing motif, where the layers are separated by an alkyl chain (the crystal stacking is shown in Fig. S1†), which makes the transfer integral between the two adjacent inter-layer molecules extremely small (around  $10^{-5}$ – $10^{-6}$  eV), which indicates that the hole transport is mainly of the intra-layer nature. The six intra-layer nearest hopping pathways for each isomer and the corresponding transfer integrals are shown in Fig. 2. The key structural parameters for these dimers are listed in Table S1.† The transfer integral depends on the center of mass (COM) distance ( $d_{\text{COM}}$ ) of the benzothiophene ring as well as the stacking mode. For instance, the transfer integral of D1 in BTBT1 with a short  $d_{\text{COM}}$  of 4.08 Å is 31.88 meV, while the transfer integral of D2 and D3 (the  $d_{\text{COM}}$  is 9.01 and 9.89 Å) is only 0.44 and 5.38 meV respectively. However, for D1 of BTBT3, although the two molecules are close in the orientation of face-to-face stacking ( $d_{\text{COM}}$  is 4.72 Å and the angle between the central rings of each monomer is  $0^\circ$ ), the transfer integral is only 5.7 meV. This is due to the phase and nodal feature of the HOMO, and the transfer integral oscillates as the molecule slips along the long or short axis.<sup>9</sup> For example, in the case of D1 of BTBT3, relative slipping of two molecules (3.17 Å along the long molecular axis and 0.28 Å along the short molecular axis) results in the small overlapping of HOMOs (Fig. S5†) and thus small transfer integral.

In the calculations, we noticed that, for BTBT1 and BTBT4, only two dimers in one direction show the maximum transfer integral value, which is several times larger than the second maximum value, thus makes the hole transport of the quasi one-dimensional (quasi-1D) nature. On the other hand, for BTBT2 and BTBT3, more than two dimers have the maximum

transfer integral value or six dimers have similar large values, and thus they behave as of the two-dimensional (2D) transport nature. Here, the hole hopping rates are evaluated by using both the Marcus theory and quantum nuclear tunneling method, and the results showed that the values by Marcus theory are smaller than those by the quantum nuclear tunneling method (the hopping rates are listed in Table S2†). Contrary to the Marcus theory, the quantum nuclear tunneling method considers the quantum effect of nuclear vibration, which can effectively reduce the barrier between the charge transfer initial state and final state, thus increasing the hopping rate.<sup>6</sup> Based on the obtained hole hopping rates, the kMC simulations without considering disorder are further performed to get the mobility in the crystal state, and the results are shown in Table 2. As expected, the mobility calculated by the quantum nuclear tunneling method is larger than that calculated by Marcus theory. For BTBT2, the average hole mobility calculated by the former method is  $2.33 \text{ cm}^2 \text{ V}^{-1} \text{ s}^{-1}$ , which is comparable to the experimental value<sup>11,16</sup> of  $0.44$ – $1.71 \text{ cm}^2 \text{ V}^{-1} \text{ s}^{-1}$ . Among the four BTBT isomers, BTBT4 has the maximum hole mobility of  $11.8 (2.34) \text{ cm}^2 \text{ V}^{-1} \text{ s}^{-1}$  evaluated by using the quantum nuclear tunneling method (Marcus theory), and this is due to the large transfer integral of D1. On the other hand, the average mobilities of BTBT1 and BTBT3 are  $0.507 (0.0914)$  and  $0.917 (0.328) \text{ cm}^2 \text{ V}^{-1} \text{ s}^{-1}$  by using the quantum nuclear tunneling method (Marcus theory), which conforms very well to the 1D and 2D transport nature.

### 3.2 Dynamic disorder in transfer integral $V$

Molecules are in constant motion, which results in the fluctuation of intermolecular transfer integral  $V$ . To account for the positional fluctuation, the MD simulations are performed to obtain the molecular position fluctuation which is subsequently used to calculate the transfer integral. The statistical results of transfer integrals for the 2050 snapshots are shown in Table 3. Results show that the average values ( $\langle V \rangle$ ) of transfer integrals are comparable to the fixed values in crystal structure. The fluctuations follow typical Gaussian distribution as shown in Fig. 3 and S7.† The standard transfer integral deviation ( $\sigma(V)$ ) is in the region of 2–41 meV. We should note that the ratio of  $\sigma(V)/\langle V \rangle$  shows a maximum value of 91 for dimer D2 in BTBT1 and a minimum value of only 0.23 for D2 in BTBT2 as shown in Table 3. For example, for D1 of BTBT1/BTBT3/BTBT4,  $\sigma(V)$  shows a comparable value in the range of 35–41 meV, while the corresponding  $\langle V \rangle$  values are 23.06, 0.93, and 138.78 meV respectively. Namely, there is no obvious cor-

**Table 2** The pure crystal mobilities of four BTBT isomers without considering disorder along  $a$ ,  $b$ , and  $c$  directions and the average values, the values are calculated by using the Marcus theory and quantum nuclear tunneling method (the unit is in  $\text{cm}^2 \text{ V}^{-1} \text{ s}^{-1}$ )

|                           |                    | BTBT-1 | BTBT-2 | BTBT-3 | BTBT-4 |
|---------------------------|--------------------|--------|--------|--------|--------|
| Marcus                    | $\mu_a$            | 0.238  | 1.610  | 0.024  | 0.000  |
|                           | $\mu_b$            | 0.036  | 0.577  | 0.093  | 6.930  |
|                           | $\mu_c$            | 0.000  | 0.000  | 0.891  | 0.086  |
|                           | $\mu_{\text{ave}}$ | 0.091  | 0.729  | 0.328  | 2.340  |
| Quantum nuclear tunneling | $\mu_a$            | 1.340  | 5.260  | 0.066  | 0.001  |
|                           | $\mu_b$            | 0.179  | 1.720  | 0.245  | 34.900 |
|                           | $\mu_c$            | 0.000  | 0.001  | 2.500  | 0.377  |
|                           | $\mu_{\text{ave}}$ | 0.507  | 2.330  | 0.917  | 11.800 |

**Table 3** The average values ( $\langle V \rangle$ , meV), standard deviation ( $\sigma$ , meV), and  $\sigma/\langle V \rangle$  for dynamic disorder of transfer integrals of four BTBT isomers at 300 K

|                               | BTBT1 |       |      | BTBT2 |       | BTBT3 |       | BTBT4  |      |
|-------------------------------|-------|-------|------|-------|-------|-------|-------|--------|------|
|                               | D1    | D2    | D3   | D1    | D2    | D1    | D2    | D1     | D2   |
| $\langle V \rangle$           | 23.06 | 0.03  | 3.89 | 24.92 | 51.96 | 0.93  | 20.47 | 138.78 | 3.43 |
| $\sigma(V)$                   | 35.79 | 2.71  | 2.50 | 23.96 | 11.94 | 40.98 | 7.07  | 35.53  | 5.83 |
| $\sigma(V)/\langle V \rangle$ | 1.55  | 91.48 | 0.64 | 0.96  | 0.23  | 43.85 | 0.35  | 0.26   | 1.70 |

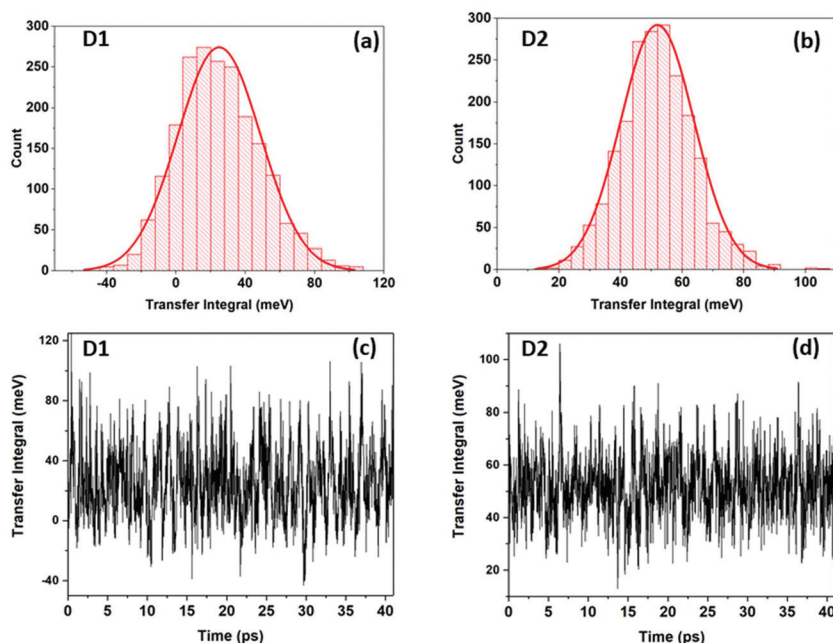


Fig. 3 The dynamic disorder of transfer integrals for BTBT2 obtained from the 2050 snapshots at 300 K. (a and b) Distribution of transfer integrals for D1/D2; (c and d) thermal fluctuation of transfer integrals for D1/D2.

relation between  $\sigma(V)$  and  $\langle V \rangle$ . For the face-to-face stacking dimers, when the molecule slips along the long or the short axis, transfer integral change resulting from oscillation leads to large fluctuation of transfer integral with small displacement, and the transfer integral can even change from negative to positive. Take D1 of BTBT3 as an example, when the slipping distance along the short axis varies from  $-1.1$  to  $1.5$  Å, the transfer integral changes from around  $-130$  meV to  $120$  meV (see Fig. 4). The  $\sigma(V)$  values for D1 and D2 of BTBT2 are 24 and 12 meV respectively as shown in Table 3, which is

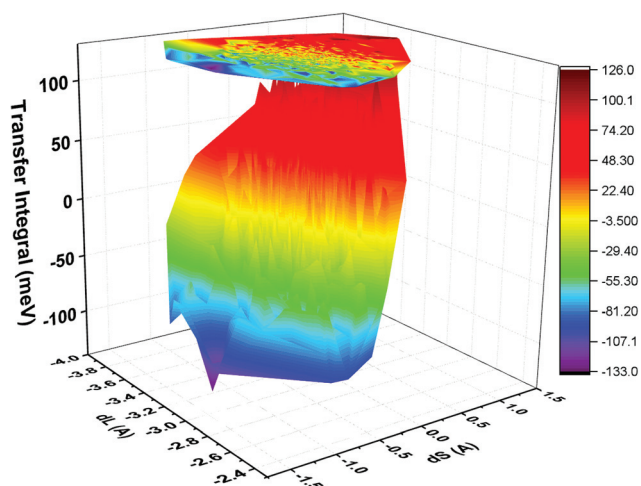


Fig. 4 The transfer integrals for D1 of BTBT3 as a function of the slipping distance along the molecular long axis ( $d_l$ ) and short axis ( $d_s$ ).

comparable to the values reported earlier (that is, 20 and 11 meV).<sup>16</sup>

Once the transfer integrals are obtained from the MD snapshots, the discrete Fourier transformation is performed to get the time-dependent transfer integral fluctuation, and then the hole transfer mobility is obtained by performing the kMC simulations. The hole mobilities by considering the dynamic disorder of transfer integrals ( $\mu(V\text{-disorder})$ ) are listed in Table 4. As the average value of transfer integrals ( $\langle V \rangle$ ) from MD snapshots may differ from the value in the crystal state, thus the mobility for the disorder-free case ( $\mu(\text{disorder-free})$ ) is calculated based on  $\langle V \rangle$ . As can be seen, by considering the dynamic disorder of transfer integrals, the  $\mu(\text{disorder})$  for the quasi-1D BTBT1 decreases slightly to a value around  $0.2 \text{ cm}^2 \text{ V}^{-1} \text{ s}^{-1}$ , which corresponds to around 80% of the value in the disorder-free case. This decrease agrees with the earlier study on pentacene by Wang *et al.*,<sup>29</sup> which indicates that dynamic disorder reduces the mobility for the 1D case and has no significant influence for the 2D case. In addition, in their study, for the 2D case, when  $\sigma(V)/\langle V \rangle$  is larger than 1, the dynamic

Table 4 Mobilities calculated by using the nuclear tunneling method for BTBT isomers by considering the dynamic disorder of transfer integrals, and the ratio of mobility with disorder  $\mu(V\text{-disorder})$  to mobility without disorder  $\mu(\text{disorder-free})$ , the unit is in  $\text{cm}^2 \text{ V}^{-1} \text{ s}^{-1}$

|       | $\mu(V\text{-disorder})$ | $\mu(V\text{-disorder})/\mu(\text{disorder-free})$ |
|-------|--------------------------|--|
| BTBT1 | 0.20                     | 0.80   |
| BTBT2 | 1.83                     | 1.08   |
| BTBT3 | 1.16                     | 1.32   |
| BTBT4 | 9.03                     | 0.98   |

disorder tends to enhance charge mobility. This is consistent with our results for 2D BTBT2 and BTBT3. For BTBT2,  $\sigma(V)/\langle V \rangle$  is around 0.96 and 0.23 for D1 and D2 respectively, and a  $\mu(\text{disorder})/\mu(\text{disorder-free})$  value of 1.08 is obtained. For BTBT3, as D1 has a large  $\sigma(V)/\langle V \rangle$  value of 43.85, the mobility with disorder increases to 1.32 times the mobility for the disorder-free case. For quasi-1D BTBT4, there exists no obvious change in mobility when changing from disorder-free to disorder (here  $\mu(\text{disorder})/\mu(\text{disorder-free})$  is 0.98), and this is due to the small disorder of D1 of BTBT4 which has a small  $\sigma(V)/\langle V \rangle$  value of 0.26.

### 3.3 Dynamic disorder of site energy

When the intramolecular vibration is taken into account, the molecular site energy also fluctuates. To account for the site energy fluctuation, the structural information is also extracted from the MD simulations. In the charge transport process, the influencing factor is the site energy difference rather than the individual site energy. For the hole transport of BTBT isomers, the site energy difference can be approximated *via* the energy difference of HOMO energy ( $\Delta E_{\text{HOMO}}$ ) based on the Koopmans' theorem. The dynamic disorder of site energy is obtained by calculating the molecular  $E_{\text{HOMO}}$  from the 2050 snapshots in this work, and  $\Delta E_{\text{HOMO}}$  is obtained from the energy difference of two randomly selected values from the 2050  $E_{\text{HOMO}}$ . Obviously, the distributions of  $E_{\text{HOMO}}$  and  $\Delta E_{\text{HOMO}}$  for each BTBT isomer are of the Gaussian type as shown in Fig. 5 and S8,<sup>†</sup> and the corresponding standard deviation of  $E_{\text{HOMO}}$  ( $\sigma(E_{\text{HOMO}})$ ) is in the range of 0.060 to 0.073 eV as shown in Table 5, which is similar to the results of 0.05–0.1 eV in polymers,  $C_{60}$ ,  $C_{70}$  and so on.<sup>9,36,37</sup> The standard deviation of  $\Delta E_{\text{HOMO}}$  ( $\sigma(\Delta E_{\text{HOMO}})$ ) falls in the region of 0.086 to 0.105 eV, and this value should be  $\sqrt{2}$  times  $\sigma(E_{\text{HOMO}})$  when the sampling is enough.

The mobilities with dynamic disorder of site energy ( $\mu(\text{SE-disorder})$ ) are summarized in Table 5 and shown in Fig. 6. For each BTBT isomer, when the dynamic disorder of site energy is considered, the mobility tends to decrease, and it is true for both the quasi-1D BTBT1 and BTBT4 and 2D BTBT2 and BTBT3. However, for quasi-1D structure, the decrease is much larger than those for the 2D case. For BTBT2,  $\mu(\text{SE-disorder})/\mu(\text{disorder-free})$  is around 0.71, while for BTBT4, it is only

**Table 5** The standard deviation of HOMO energies from 2050 MD snapshots, standard deviation of HOMO energy differences for 100 000 samplings, and mobilities calculated with the nuclear tunneling method by considering the dynamic disorder of site energy, and the ratio of mobility with disorder ( $\mu(\text{SE-disorder})$ ) to mobility without disorder ( $\mu(\text{disorder-free})$ )

|       | $\sigma(E_{\text{HOMO}})$<br>(eV) | $\sigma(\Delta E_{\text{HOMO}})$<br>(eV) | $\mu(\text{SE-disorder})$<br>( $\text{cm}^2 \text{V}^{-1} \text{s}^{-1}$ ) | $\mu(\text{SE-disorder})/\mu(\text{disorder-free})$ |
|-------|-----------------------------------|--|--|---|
| BTBT1 | 0.060                             | 0.086                                    | 0.15   | 0.31  |
| BTBT2 | 0.073                             | 0.105                                    | 1.66   | 0.71  |
| BTBT3 | 0.065                             | 0.092                                    | 0.64   | 0.70  |
| BTBT4 | 0.061                             | 0.086                                    | 2.33   | 0.20  |

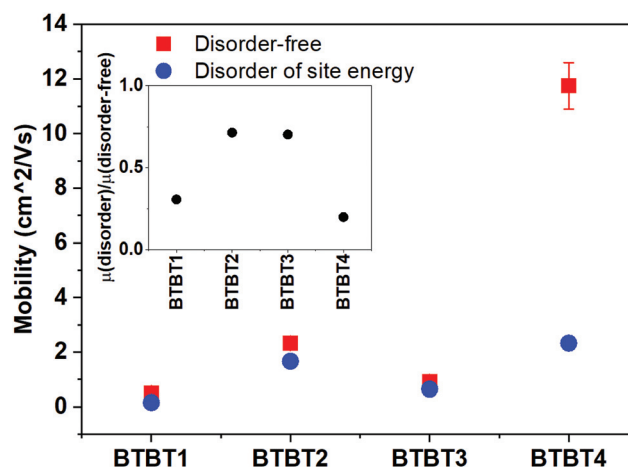


**Fig. 6** Mobilities of four BTBT isomers with dynamic disorder of site energy (blue dot), and those without dynamic disorder of site energy (red square). The inset shows the ratios of mobilities for isomers with disorder to those for isomers without disorder.

around 0.2. In a KMC process, assuming that each site has  $n$  equal-rate hopping pathways, and the rate of each pathway is  $k$ , thus the rate of one hopping step ( $k_n$ ) is the sum of these  $n$  rates. However, in a dynamic disorder system, the rates for each hopping step may vary, as a result the mean hopping rate can be expressed as a harmonic mean ( $H_{k_n}$ ) of all the  $k_n$  values of each step. As the mobility is positively correlated to  $H_{k_n}$ , we can use the ratio of  $H_{k_n}$  to disorder-free  $k_n$  ( $k_n^{\text{disorder-free}}$ ),

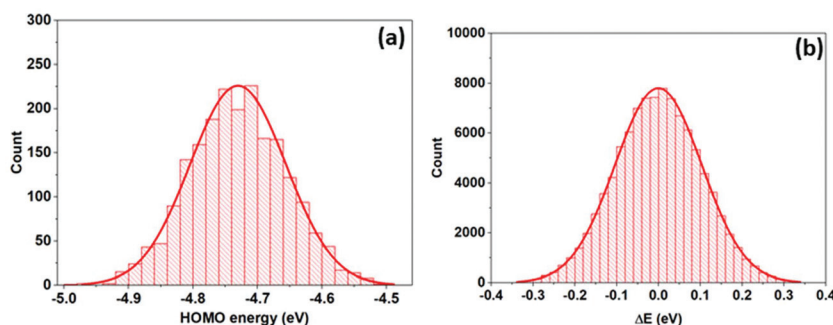


**Fig. 5** Distribution of (a) HOMO energy of BTBT2 from the 2050 snapshots and (b) energy difference of BTBT2 HOMO from 100 000 samplings.

$H_{k_n}/k_n^{\text{disorder-free}}$ , to reflect the influence of dynamic disorder on mobility. Based on the hopping rates of BTBT4 D1, after performing 100 000 hopping steps at different  $n$ , we found that  $H_{k_n}/k_n^{\text{disorder-free}}$  increases with  $n$ , and at the same time,  $H_{k_n}/n$  is approaching the mean value of  $k$  ( $\langle k \rangle$ ) as shown in Fig. S9.† For the 1D case, we have  $n = 2$ , and the corresponding  $H_{k_n}/k_n^{\text{disorder-free}}$  is around 0.149, which is smaller than  $\mu(\text{SE-disorder})/\mu(\text{disorder-free})$  of BTBT4 (around 0.2). This discrepancy is due to the more than 2 hopping pathways (e.g. the slower D2) in BTBT4. As  $n$  increases,  $H_{k_n}/k_n^{\text{disorder-free}}$  gradually approaches  $n \cdot \langle k \rangle / k_n^{\text{disorder-free}}$  or  $\langle k \rangle / k^{\text{disorder-free}}$ , where  $k^{\text{disorder-free}}$  is the hop rate of a path when  $\Delta G = 0$ . However, it should be noted that  $\langle k \rangle / k^{\text{disorder-free}}$  can be smaller or larger than 1. Based on Marcus theory,  $\langle k \rangle$  is larger than  $k^{\text{disorder-free}}$ , and we found that mobilities for 2D BTBT2 and BTBT3 with site energy disorder are larger than those without site energy disorder as shown in Table S4.† As the Marcus rate is in an exponential form, in the range around  $\Delta G = 0$ , the absolute value of the derivative of hopping rates increases with a decrease in  $\Delta G$  (an example of BTBT2 D2 is shown in Fig. S10†), as a result  $\langle k \rangle$  (for a Gaussian distribution of  $\Delta G$ ) is larger than the  $k$  value at  $\Delta G = 0$ .

### 3.4 Static disorder of defects

Defects are inevitable in the preparation of organic semiconductor materials, and even in the case of rubrene and pentacene organic single crystals which feature high-mobility,<sup>58–60</sup> the trap defects can be found with a density of  $\sim 10^{15}$ – $10^{18}$   $\text{cm}^{-3}$ . In organic semiconductors, defects exist in various

forms, it may be that a different chemical structure resulted from the side products of a chemical synthesis or chemical reactions with oxygen or water,<sup>8</sup> for example, a pentacene-quinone molecule was found in a pentacene single crystal.<sup>42</sup> For the hole transport in this work, when the HOMO energy of a defect ( $E_{\text{defect}}$ ) is located higher than that of the normal molecule, the defect would act as a trap, otherwise it would act as a scatter. Here, two types of defects with different energies are considered to evaluate the mobilities at an applied electric field of  $10^6$   $\text{V cm}^{-1}$ . A typical 2D BTBT2 and a quasi-1D BTBT4 are chosen to investigate the influence of defects on mobilities for the 2D and 1D stacking structures, and evolution of mobility are shown in Fig. 7. As can be seen, in a certain range, for both the trap and scatter defects, as the absolute value of energy difference ( $\Delta G$ ) between defect and normal molecule increases, the mobility decreases. In the case of trap defects (Fig. 7(a) and (c)), the mobility drops abruptly when  $\Delta G$  increases beyond a threshold value of about 100 meV, this phenomenon is also observed in the earlier study on 1D pentacene.<sup>61</sup> Beyond a threshold value, the mobility decreases exponentially with an increase in  $\Delta G$ . On the other hand, in the case of the scatter defects (Fig. 7(b) and (d)), mobility decreases monotonously with a decrease in  $\Delta G$ , and then it stabilizes when  $\Delta G$  is lower than a threshold value of about  $-200$  meV. Compared to the scatter defect, the trap defect can induce to more significant reduction in mobility, especially when the energy difference between the defect and a normal molecule is large. As expected, mobility decreases with an increase in defect ratio for the two types of defects.

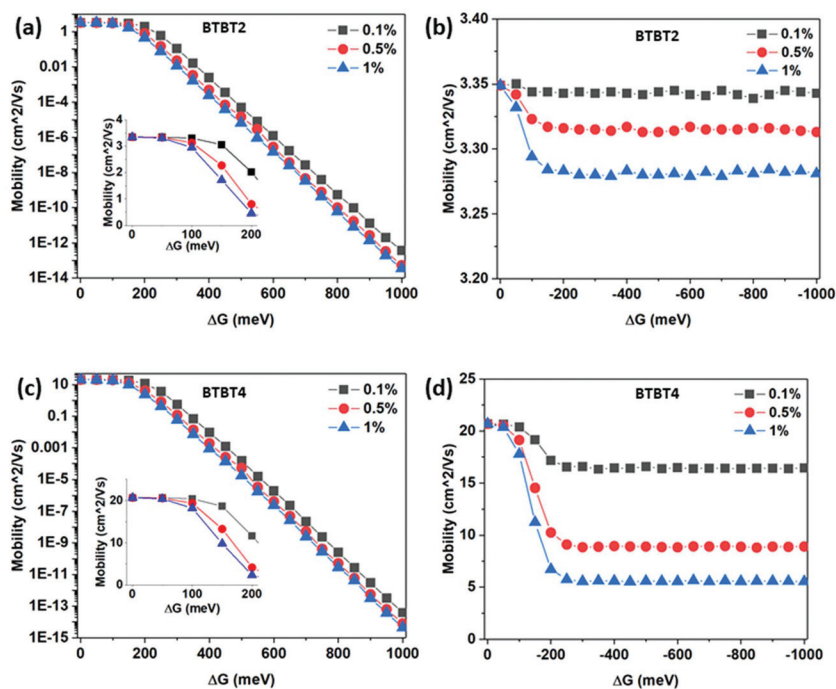


Fig. 7 Evolution of mobility as a function of  $\Delta G$  (difference between HOMO energies of defect and normal molecule) at an applied electric field of  $10^6$   $\text{V cm}^{-1}$  with different defect ratios. (a and c) Mobilities as a function of trap defects for BTBT2 and BTBT4 respectively, and the inset shows that mobility changes with  $\Delta G$  in the range of 0 to 200 meV; (b and d) mobilities as a function of scatter defects for BTBT2 and BTBT4 respectively.

As is known that thiophene can be oxidized to form thiophene 1-oxides (one oxygen atom substituted on a sulfur atom) or thiophene 1,1-dioxides (two oxygen atoms substituted on a sulfur atom) in the presence of water and oxygen.<sup>62</sup> Thus, we can reasonably assume that these BTBT isomer crystals may contain defects such as BTBT-oxides (one oxygen atom attached on each sulfur atom) or BTBT-dioxides (two oxygen atoms attached on each sulfur atom) (the chemical structures for BTBT2 and BTBT4 are shown in Fig. 8). Both the BTBT-oxides and BTBT-dioxides are characterized as scatter defects, and the corresponding  $\Delta G$  are in the range of  $-550$ – $-680$  meV and  $-900$ – $-1000$  meV, respectively (Table S5<sup>†</sup>). Due to the large absolute values of  $\Delta G$ , as discussed above, the influence on mobility for these two types of defects should be similar (Fig. 7(b) and (d)). The mobility distributions for BTBT2 and BTBT4 at various defect ratios (with  $\Delta G$  set to  $-600$  meV) are summarized in Table 6 and shown in Fig. 9. For 2D BTBT2, the mobility exhibits no obvious change even though the defect ratio goes up to 1%; however, when the defect ratio goes up to 10%, the mobility decreases by 23% compared to the defect-free case. While for the quasi-1D BTBT4, on the other hand, as the defect ratio increases, reduction in mobility is much more obvious, even a small defect ratio of 0.1% could lead to 20% reduction in mobility, more reduction in mobility

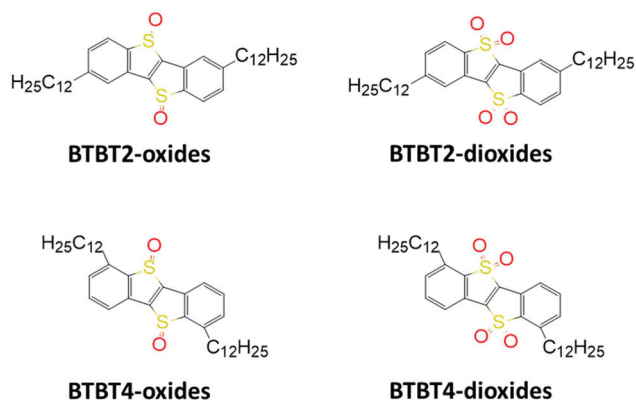


Fig. 8 The chemical structures of typical oxidized defects for BTBT2 and BTBT4.

Table 6 At an applied electric field of  $10^6$  V cm<sup>-1</sup>, mobilities  $\mu$  (cm<sup>2</sup> V<sup>-1</sup> s<sup>-1</sup>) for BTBT2 and BTBT4 at various defect ratios (the defect HOMO energy is set to 600 meV lower than the normal molecular HOMO energy)

| Defect ratio | BTBT2                 |  | BTBT4                 |  |
|--------------|-----------------------|--|-----------------------|--|
|              | $\mu_{\text{defect}}$ | $\mu_{\text{defect}}/\mu_{\text{defect-free}}$ | $\mu_{\text{defect}}$ | $\mu_{\text{defect}}/\mu_{\text{defect-free}}$ |
| 0.00%        | 3.35                  | 1.00   | 20.69                 | 1.00   |
| 0.01%        | 3.35                  | 1.00   | 20.14                 | 0.97   |
| 0.10%        | 3.34                  | 1.00   | 16.46                 | 0.80   |
| 0.50%        | 3.32                  | 0.99   | 8.84                  | 0.43   |
| 1.00%        | 3.28                  | 0.98   | 5.56                  | 0.27   |
| 5.00%        | 3.00                  | 0.89   | 1.19                  | 0.06   |
| 10.00%       | 2.59                  | 0.77   | 0.46                  | 0.02   |

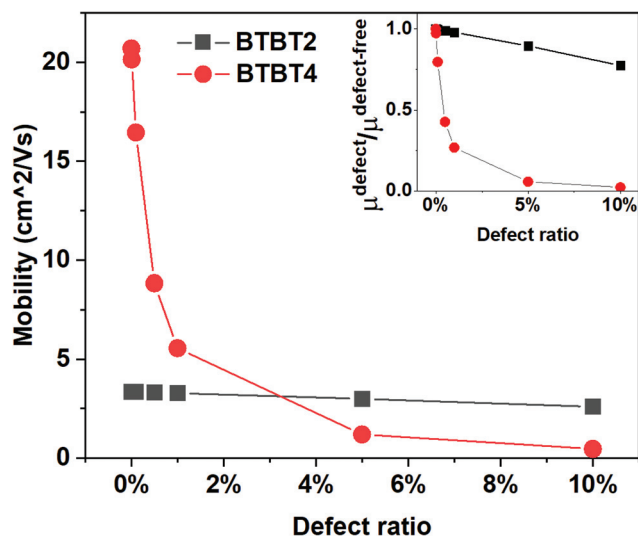


Fig. 9 Mobilities for BTBT2 and BTBT4 as a function of defect ratio ( $\Delta G$  is set to  $-600$  meV) at an applied electric field of  $10^6$  V cm<sup>-1</sup>. The inset shows the ratio of mobility with defects to mobility without defects.

may occur by further increasing the defect ratio, for example, 1% defect ratio can lead to 73% reduction in mobility, while 10% defect ratio can lead to 98% reduction in mobility.

For the 2D case, when a hole carrier hops forward in a channel and encounters a scatter defect, if the hopping rate to an adjacent channel ( $k^{\text{adjacent}}$ ) is at maximum, then it prefers to hop to the adjacent channel and continue the forward jumping, and mobility decreases as  $k^{\text{adjacent}}$  decreases. If  $k^{\text{adjacent}}$  is small enough and less than the backwards hopping rate, then the hole carrier prefers to hop back and forth repeatedly, and this is actually a trap that could lead to a much more reduced mobility. The quasi-1D packing motif (e.g., BTBT4 in this work) corresponds to such a case.

## 4. Conclusion

We have applied a multiscale approach by combining molecular dynamics simulations, quantum mechanics calculations and kinetic Monte-Carlo simulations to investigate the influence of dynamic and static disorder on the hole mobilities of four BTBT isomers.

The dynamic off-diagonal disorder that reflects the fluctuation of transfer integral incurs a decrease in mobility for quasi-1D BTBT1 and BTBT4, while it tends to result in an increase in mobility for the 2D BTBT2 and BTBT3 cases. In addition, the results showed that the face-to-face  $\pi$ - $\pi$  stacking tends to induce a large fluctuation of transfer integral, with the standard deviation in the range of 35–40 meV. For the 2D packing motif, if dimers are of the face-to-face  $\pi$ - $\pi$  stacking and the corresponding transfer integrals are small (e.g., D1 of BTBT3), the dynamic disorder could enhance mobility markedly, as the intermolecular motions can result in a significant increase in transfer integral.

The dynamic diagonal disorder that reflects that the site energy fluctuation leads to a decrease in mobility for all the four BTBT isomers, but the reduction is much more obvious for the quasi-1D BTBT1 and BTBT4 cases than for the 2D BTBT2 and BTBT3 cases. Contrary to the 1D case, the 2D molecule structure has more hopping paths and tends to weaken the hopping rate fluctuation, and thus shows less reduction in mobility.

Incorporation of the static disorder of the defect tends to decrease mobility. The trap defect tends to result in a decrease in mobility exponentially with an increase in defect energy when the defect energy is higher than a certain threshold value, while the scatter defect tends to result in a limited reduction in mobility. The abovementioned two oxidation defects are of the scatter type, and reduction in mobility for quasi-1D BTBT4 is much more severe than that for 2D BTBT2 with increasing defect ratio.

It is generally believed that the FET structure measures a few layers of molecules close to the substrate, while the Hall measurement requires substantially larger size for the bulk transport behavior. So, for many materials, FET mobility is larger than Hall mobility, namely, impurities inside the materials might be swept out by the gate voltage. However, for the well-ordered high mobility systems, both are close to each other. We thus speculate that the value with the dynamic disorder and without the static disorder should be close to FET mobility and the values with both static and dynamic disorder should be the Hall mobility.

In general, both dynamic and static disorder are more detrimental for the quasi-1D molecular structure than for the 2D molecular structure. The reduction in mobility induced by the dynamic disorder and scatter defect is normally restricted within an order of magnitude, while the trap defect tends to result in significant reduction in mobility which could be up to several orders of magnitude. As a result, in reality, dynamic and static disorder are inevitable in organic materials; in the aspect of charge transport, the 2D structure is almost always favored over the quasi-1D or 1D structure, which may provide a good clue to devise design in organic electronics.

## Conflicts of interest

There are no conflicts to declare.

## Acknowledgements

This work is supported by the National Natural Science Foundation of China through the project “Science Center for Luminescence from Molecular Aggregates” (SCELMA) (Grant No. 21788102) as well as by the Ministry of Science and Technology of China through the National Key R&D Plan, Grant No. 2017YFA0204501.

## References

- 1 H. Chen, W. Zhang, M. Li, G. He and X. Guo, *Chem. Rev.*, 2020, **120**, 2879–2949.
- 2 S. E. Root, S. Savagatrup, A. D. Printz, D. Rodriguez and D. J. Lipomi, *Chem. Rev.*, 2017, **117**, 6467–6499.
- 3 C. Wang, H. Dong, L. Jiang and W. Hu, *Chem. Soc. Rev.*, 2018, **47**, 422–500.
- 4 H. Oberhofer, K. Reuter and J. Blumberger, *Chem. Rev.*, 2017, **117**, 10319–10357.
- 5 L. Wang, G. Nan, X. Yang, Q. Peng, Q. Li and Z. Shuai, *Chem. Soc. Rev.*, 2010, **39**, 423–434.
- 6 Z. Shuai, H. Geng, W. Xu, Y. Liao and J. M. Andre, *Chem. Soc. Rev.*, 2014, **43**, 2662–2679.
- 7 Y. Jiang, H. Geng, W. Li and Z. Shuai, *J. Chem. Theory Comput.*, 2019, **15**, 1477–1491.
- 8 O. Ostroverkhova, *Chem. Rev.*, 2016, **116**, 13279–13412.
- 9 V. Coropceanu, J. Cornil, D. A. da Silva Filho, Y. Olivier, R. Silbey and J. L. Bredas, *Chem. Rev.*, 2007, **107**, 926–952.
- 10 S. Fratini, M. Nikolka, A. Salleo, G. Schweicher and H. Sirringhaus, *Nat. Mater.*, 2020, **19**, 491–502.
- 11 H. Ebata, T. Izawa, E. Miyazaki, K. Takimiya, M. Ikeda, H. Kuwabara and T. Yui, *J. Am. Chem. Soc.*, 2007, **129**, 15732–15733.
- 12 D. He, Y. Zhang, Q. Wu, R. Xu, H. Nan, J. Liu, J. Yao, Z. Wang, S. Yuan, Y. Li, Y. Shi, J. Wang, Z. Ni, L. He, F. Miao, F. Song, H. Xu, K. Watanabe, T. Taniguchi, J. B. Xu and X. Wang, *Nat. Commun.*, 2014, **5**, 5162.
- 13 T. Uemura, K. Nakayama, Y. Hirose, J. Soeda, M. Uno, W. Li, M. Yamagishi, Y. Okada and J. Takeya, *Curr. Appl. Phys.*, 2012, **12**, S87–S91.
- 14 Y. Yuan, G. Giri, A. L. Ayzner, A. P. Zoombelt, S. C. Mannsfeld, J. Chen, D. Nordlund, M. F. Toney, J. Huang and Z. Bao, *Nat. Commun.*, 2014, **5**, 3005.
- 15 H. Iino, T. Usui and J. Hanna, *Nat. Commun.*, 2015, **6**, 6828.
- 16 Y. Tsutsui, G. Schweicher, B. Chattopadhyay, T. Sakurai, J. B. Arlin, C. Ruzie, A. Aliev, A. Ciesielski, S. Colella, A. R. Kennedy, V. Lemaury, Y. Olivier, R. Hadji, L. Sanguinet, F. Castet, S. Osella, D. Dudenko, D. Beljonne, J. Cornil, P. Samori, S. Seki and Y. H. Geerts, *Adv. Mater.*, 2016, **28**, 7106–7114.
- 17 T. Izawa, E. Miyazaki and K. Takimiya, *Adv. Mater.*, 2008, **20**, 3388–3392.
- 18 M. Alkan and I. Yavuz, *Phys. Chem. Chem. Phys.*, 2018, **20**, 15970–15979.
- 19 A. S. Eggeman, S. Illig, A. Troisi, H. Sirringhaus and P. A. Midgley, *Nat. Mater.*, 2013, **12**, 1045–1049.
- 20 A. Troisi and G. Orlandi, *J. Phys. Chem. A*, 2006, **110**, 4065–4070.
- 21 H. Geng, Q. Peng, L. Wang, H. Li, Y. Liao, Z. Ma and Z. Shuai, *Adv. Mater.*, 2012, **24**, 3568–3572.
- 22 S. Illig, A. S. Eggeman, A. Troisi, L. Jiang, C. Warwick, M. Nikolka, G. Schweicher, S. G. Yeates, Y. Henri Geerts, J. E. Anthony and H. Sirringhaus, *Nat. Commun.*, 2016, **7**, 10736.

- 23 T. Kubo, R. Hausermann, J. Tsurumi, J. Soeda, Y. Okada, Y. Yamashita, N. Akamatsu, A. Shishido, C. Mitsui, T. Okamoto, S. Yanagisawa, H. Matsui and J. Takeya, *Nat. Commun.*, 2016, **7**, 11156.
- 24 K. Sakai, Y. Okada, T. Uemura, J. Tsurumi, R. Häusermann, H. Matsui, T. Fukami, H. Ishii, N. Kobayashi, K. Hirose and J. Takeya, *NPG Asia Mater.*, 2016, **8**, e252–e252.
- 25 Z. Shuai, W. Li, J. Ren, Y. Jiang and H. Geng, *J. Chem. Phys.*, 2020, **153**, 080902.
- 26 S. Giannini, A. Carof, M. Ellis, H. Yang, O. G. Zigos, S. Ghosh and J. Blumberger, *Nat. Commun.*, 2019, **10**, 3843.
- 27 L. Song and Q. Shi, *J. Chem. Phys.*, 2015, **142**, 174103.
- 28 L. Wang and D. Beljonne, *J. Phys. Chem. Lett.*, 2013, **4**, 1888–1894.
- 29 L. Wang, Q. Li, Z. Shuai, L. Chen and Q. Shi, *Phys. Chem. Chem. Phys.*, 2010, **12**, 3309–3314.
- 30 H. Bässler, *Phys. Status Solidi B*, 1993, **175**, 15–56.
- 31 P. Kordt and D. Andrienko, *J. Chem. Theory Comput.*, 2016, **12**, 36–40.
- 32 A. Miller and E. Abrahams, *Phys. Rev.*, 1960, **120**, 745–755.
- 33 R. A. Marcus, *Rev. Mod. Phys.*, 1993, **65**, 599–610.
- 34 I. I. Fishchuk, A. Kadashchuk, H. Bässler and M. Abkowitz, *Phys. Rev. B: Condens. Matter Mater. Phys.*, 2004, **70**, 245212.
- 35 H. Bassler and A. Kohler, *Top. Curr. Chem.*, 2012, **312**, 1–65.
- 36 N. R. Tummala, Z. Zheng, S. G. Aziz, V. Coropceanu and J. L. Bredas, *J. Phys. Chem. Lett.*, 2015, **6**, 3657–3662.
- 37 P. de Silva and T. Van Voorhis, *J. Phys. Chem. Lett.*, 2018, **9**, 1329–1334.
- 38 L. G. Kaake, P. F. Barbara and X. Y. Zhu, *J. Phys. Chem. Lett.*, 2010, **1**, 628–635.
- 39 J. H. Kang, D. da Silva Filho, J.-L. Bredas and X. Y. Zhu, *Appl. Phys. Lett.*, 2005, **86**, 152115.
- 40 R. K. Hallani, K. J. Thorley, Y. Mei, S. R. Parkin, O. D. Jurchescu and J. E. Anthony, *Adv. Funct. Mater.*, 2016, **26**, 2341–2348.
- 41 P. J. Diemer, J. Hayes, E. Welchman, R. Hallani, S. J. Pookpanratana, C. A. Hacker, C. A. Richter, J. E. Anthony, T. Thonhauser and O. D. Jurchescu, *Adv. Funct. Mater.*, 2017, **3**, 1600294.
- 42 O. D. Jurchescu, J. Baas and T. T. M. Palstra, *Appl. Phys. Lett.*, 2004, **84**, 3061–3063.
- 43 N. von Malm, J. Steiger, R. Schmechel and H. von Seggern, *J. Appl. Phys.*, 2001, **89**, 5559–5563.
- 44 B. Li, J. Chen, Y. Zhao, D. Yang and D. Ma, *Org. Electron.*, 2011, **12**, 974–979.
- 45 H. T. Nicolai, M. Kuik, G. A. Wetzelaer, B. de Boer, C. Campbell, C. Risko, J. L. Bredas and P. W. Blom, *Nat. Mater.*, 2012, **11**, 882–887.
- 46 G. Zuo, M. Linares, T. Upreti and M. Kemerink, *Nat. Mater.*, 2019, **18**, 588–593.
- 47 E. F. Valeev, V. Coropceanu, D. A. da Silva Filho, S. Salman and J. L. Bredas, *J. Am. Chem. Soc.*, 2006, **128**, 9882–9886.
- 48 Y. Niu, W. Li, Q. Peng, H. Geng, Y. Yi, L. Wang, G. Nan, D. Wang and Z. Shuai, *Mol. Phys.*, 2018, **116**, 1078–1090.
- 49 M. J. Frisch, G. W. Trucks, H. B. Schlegel, G. E. Scuseria, M. A. Robb, J. R. Cheeseman, G. Scalmani, V. Barone, B. Mennucci, G. A. Petersson, H. Nakatsuji, M. Caricato, X. Li, H. P. Hratchian, A. F. Izmaylov, J. Bloino, G. Zheng, J. L. Sonnenberg, M. Hada, M. Ehara, K. Toyota, R. Fukuda, J. Hasegawa, M. Ishida, T. Nakajima, Y. Honda, O. Kitao, H. Nakai, T. Vreven, J. A. Montgomery Jr., J. E. Peralta, F. Ogliaro, M. Bearpark, J. J. Heyd, E. Brothers, K. N. Kudin, V. N. Staroverov, T. Keith, R. Kobayashi, J. Normand, K. Raghavachari, A. Rendell, J. C. Burant, S. S. Iyengar, J. Tomasi, M. Cossi, N. Rega, J. M. Millam, M. Klene, J. E. Knox, J. B. Cross, V. Bakken, C. Adamo, J. Jaramillo, R. Gomperts, R. E. Stratmann, O. Yazyev, A. J. Austin, R. Cammi, C. Pomelli, J. W. Ochterski, R. L. Martin, K. Morokuma, V. G. Zakrzewski, G. A. Voth, P. Salvador, J. J. Dannenberg, S. Dapprich, A. D. Daniels, O. Farkas, J. B. Foresman, J. V. Ortiz, J. Cioslowski and D. J. Fox, *Gaussian 09, Revision E.01*, Gaussian, Inc., Wallingford CT, 2013.
- 50 J. Wang, R. M. Wolf, J. W. Caldwell, P. A. Kollman and D. A. Case, *J. Comput. Chem.*, 2004, **25**, 1157–1174.
- 51 C. I. Bayly, P. Cieplak, W. Cornell and P. A. Kollman, *J. Phys. Chem.*, 1993, **97**, 10269–10280.
- 52 T. Fox and P. A. Kollman, *J. Phys. Chem. B*, 1998, **102**, 8070–8079.
- 53 M. J. Abraham, T. Murtola, R. Schulz, S. Páll, J. C. Smith, B. Hess and E. Lindahl, *SoftwareX*, 2015, **1–2**, 19–25.
- 54 G. Han, X. Shen, R. Duan, H. Geng and Y. Yi, *J. Mater. Chem. C*, 2016, **4**, 4654–4661.
- 55 G. Han, Y. Guo, R. Duan, X. Shen and Y. Yi, *J. Mater. Chem. A*, 2017, **5**, 9316–9321.
- 56 G. Bussi, D. Donadio and M. Parrinello, *J. Chem. Phys.*, 2007, **126**, 014101.
- 57 H. J. C. Berendsen, J. P. M. Postma, W. F. van Gunsteren, A. DiNola and J. R. Haak, *J. Chem. Phys.*, 1984, **81**, 3684–3690.
- 58 C. Krellner, S. Haas, C. Goldmann, K. P. Pernstich, D. J. Gundlach and B. Batlogg, *Phys. Rev. B: Condens. Matter Mater. Phys.*, 2007, **75**, 245115.
- 59 J. Dacuña and A. Salleo, *Phys. Rev. B: Condens. Matter Mater. Phys.*, 2011, **84**, 195209.
- 60 J. Dacuña, W. Xie and A. Salleo, *Phys. Rev. B: Condens. Matter Mater. Phys.*, 2012, **86**, 115202.
- 61 Y. Olivier, V. Lemaire, J. L. Bredas and J. Cornil, *J. Phys. Chem. A*, 2006, **110**, 6356–6364.
- 62 Y. Lu, Z. Dong, P. Wang and H.-B. Zhou, in *Thiophenes*, ed. J. A. Joule, Springer International Publishing, Cham, 2015, pp. 227–293, DOI: 10.1007/7081\_2014\_132.